Quantum Electronics **52** (4) 313–321 (2022)

https://doi.org/10.1070/QEL18024

Nonlinear phenomena in femtosecond laser systems based on Yb:YAG thin-rod amplifiers

J.W. Kim, S. Park, E.G. Sall, G.-H. Kim, V.E. Yashin, J. Yang

Abstract. **Nonlinear effects in a high-power laser amplification system based on thin-rod active elements are experimentally investigated. It is shown that the most important nonlinear effect is the Kerr effect leading to self-focusing and self-phase modulation of laser radiation. The observed luminescence in Yb:YAG crystals in the visible region of the spectrum is caused by the charge transfer luminescence effect, which, in turn, is due to multiphoton absorption of laser radiation. Second-order nonlinearity in the crystal is used to effectively convert femtosecond pulses to second harmonic and sum-frequency waves which exhibit radiations of green and UV spectra.**

Keywords: *nonlinear phenomena, thin rods, Yb: YAG, Kerr effect, self-focusing, self-phase modulation, femtosecond laser pulses, high power laser system.*

1. Introduction

Various nonlinear optical effects play a very important role in the generation and amplification of ultrashort laser pulses, as well as in the transformation of their frequency and space-time structure. The second and third-order nonlinear optical properties give rise to a large variety of optical phenomena. The second-order susceptibility is responsible for second harmonic generation, sum and difference frequency generation, optical rectification, Pockels effect, and optical parametric amplification. The third-order optical nonlinearities govern third-harmonic generation, optical Kerr effect, four-wave mixing, Raman scattering, Brillouin scattering, and optical phase conjugation [1, 2].

Many of these effects are fully manifested in laser systems with a high peak radiation power and an ultrashort pulse duration. Recently, the attention of researchers has been attracted by laser systems based on thin-rod active elements [3–5]. These lasers, in which Yb:YAG is the active medium, are capable of operating at high pulse repetition rates and high peak and average powers, which makes them attractive for a variety of applications. This paper presents the results of a study of various nonlinear effects in a femtosecond laser system based on thin-rod Yb:YAG active elements [6, 7]. The following effects are considered: self-focusing by the Kerr lens effect, spectral broadening by self-phase modulation, and charge transfer luminescence by multiphoton absorption. The results of research on the frequency conversion of femtosecond pulses using quadratic nonlinear media are presented.

J.W. Kim, S. Park, E.G. Sall, G.-H. Kim, J. Yang Electro-Medical Device Research Center, Korea Electrotechnology Research Institute, 111, Hanggaul-ro, Sangnok-gu, Ansan-si, Gyeonggi-do, 15588, Republic of Korea; e-mail: zuee@keri.re.kr;
V.E. Yashin ITMO University, Kronverksky prosp. 49, 197101 St. Petersburg, Russia; e-mail: Vladimir_Yashin@mail.ru

Received 1 December 2021
Kvantovaya Elektronika **52** (4) 313–321 (2022)
Submitted in English

2. Kerr effects and charge transfer luminescence with a Yb:YAG thin-rod fs amplifiers

Ytterbium-doped YAG is one of the most widely used crystals for high-power femtosecond lasers and amplifiers. This choice is due to its beneficial optical performance (e.g., good thermal conductivity and wide emission cross-section), which can be used specially for generation and amplification of ultrafast pulses. For ultrashort pulse amplification, a thin-rod with a diameter less than 1 mm and a typical length of a few centimetres provides several advantages. These include simple, robust, and cost-effective use, along with high energy performance [3–5].

We recently developed a three-stage thin-rod amplifier (TRA) system based on a Yb:YAG crystal with chirped-pulse amplification (CPA) [7]. Femtosecond pulses were directly amplified to a 100 W average power with a 0.25–1 MHz repetition rate and a pulse duration below 950 fs. The peak power was limited by nonlinear effects, such as self-focusing, due to pulse confinement in a small cross-section element. Even though the pulses were prolonged to 50 ps, the thin-rod active medium was damaged at an approximately 5 MW peak power. Crystal damage through dramatic self-focusing can happen if the length of the active medium is greater than the critical self-focusing length z_{sf}, calculated as shown below:

$$z_{sf} = \frac{\pi d^2}{\lambda(\sqrt{P_p/P_{cr} - 1} - \theta)}, \quad (1)$$

where d is the beam diameter; λ is the wavelength in free space; P_p is the peak power of the pulse; P_{cr} is the critical power of a nonlinear medium; and θ is the beam divergence [1, 8]. Because the length of a thin-rod type laser medium is relatively long compared to that of the bulk crystal, it is very important to understand the nonlinear phenomena occurring in this nonlinear medium.

In this section, we present the results of an experimental study of several nonlinear phenomena observed in a femtosecond laser system based on a Yb:YAG thin-rod crystal and related to third-order nonlinearity. These nonlinear phenomena include, for example, self-focusing, self-phase modulation, and multiphoton absorption. To maximise the nonlin-

earity that can occur in the thin rod, the system was configured without using the CPA technique and the pulse energy was increased by reducing the pulse repetition rate. The nonlinear threshold at which self-focusing becomes serious due to the Kerr-lens effect was measured experimentally and compared with critical power and the *B*-integral. The broadened spectra that resulted from the self-phase modulations are discussed qualitatively, and phenomena revealed by an investigation of charge transfer (CT) luminescence generated by multiphoton absorption are considered.

The optical configuration of a laser system including two amplification stages based on a Yb:YAG thin rod is shown schematically in Fig. 1. The system is composed of a master oscillator (MO), a pulse picker based on a Pockels cell, a first amplification stage (operated in a double-pass scheme), and a second amplification stage (with a single-pass scheme). The master oscillator based on Yb:KGW provides 150 fs pulses at a repetition rate of 80 MHz with an average power of 2.6 W and a spectral width of 7.6 nm (FWHM) centred at a wavelength of 1030 nm. The pulse repetition rate is maintained in the range from 250 kHz to 80 MHz using a Pockels cell based on a BBO crystal operating in a double-pass regime.

The first amplifier operated in a double-pass scheme with a quarter-wave plate is based on a Yb:YAG thin-rod crystal (Shasta) with a 2.5 at.% doping rate, 1 mm diameter, and 15 mm length. It was developed at the Institute of Applied Physics of the Russian Academy of Sciences (IAP RAS). The second amplifier (with single-pass operation) is based on a 2 at.% Yb:YAG thin rod with a diameter of 1 mm and a length of 19 mm.

Both amplifiers were end-pumped with a 105 μm fibre-coupled laser diode (JDSU) with a maximum output power of 150 W at 940 nm. The pump beam and the seed beam were focused to a spot with ~300 μm diameters inside of the thin-rod active element. Several Faraday isolators were installed to prevent self-excitation of the system.

Figure 2a shows the measured output power from the second amplifier with a single-pass scheme as a function of the pump power used for pulse repetition rates of 250 kHz, 500 kHz, and 1 MHz. The maximum amplified average power is 19 W at 111 W of the pump power, with a 1 MHz repetition rate. In the case of 500 and 250 kHz, the output power is limited by a nonlinear effect because the pulse energy at the same output power increases as the pulse repetition rate is lowered. This is clear when considering the dependences of the output energy and peak power on the pump power depicted in Fig. 2b. The three horizontal dotted lines correspond to the peak powers; the different nonlinear phenomena are indicated by: (i) the threshold of self-focusing, (ii) self-phase modulation, and (iii) the charge transfer luminescence.

When ultrashort pulses propagate through a nonlinear medium, a nonlinear optical effect called the Kerr effect can occur. It is an intensity-dependent change in the refractive index for a high intensity light beam, which leads to self-focusing due to Kerr lensing and self-phase modulation. The self-focusing sets a limit on amplification of the laser power because the beam can undergo collapse in an active material that acts as a positive lens, causing optical damage to the crystal. In the absence of significant dispersion, this effect can occur when the optical power is above the critical power P_{cr}, which has the approximate form

$$P_{cr} = 0.148\frac{\lambda^2}{n_0 n_2}, \tag{2}$$

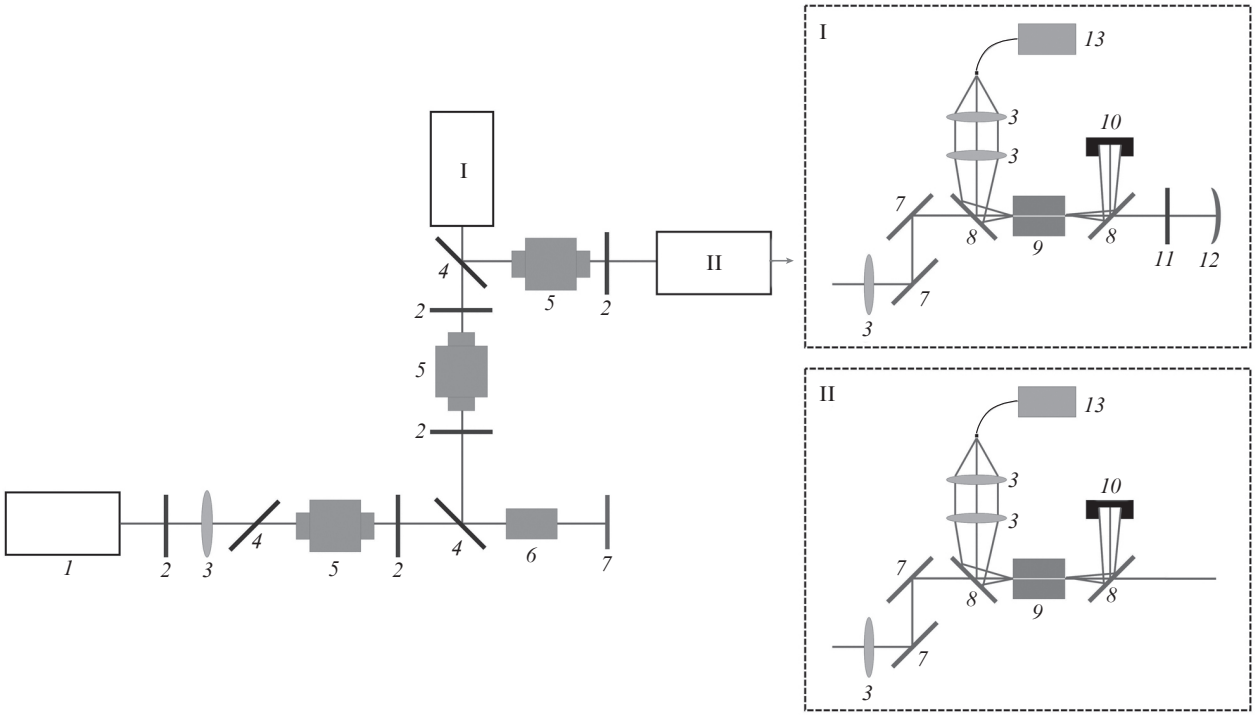

Figure 1. Schematic of the femtosecond laser system with a Yb:YAG thin-rod amplifier [(I) first double-pass amplification stages, (II) second single-pass amplification stage]:
(*1*) Yb:KGW MO; (*2*) half-wave plates; (*3*) lenses; (*4*) thin film polarisers; (*5*) Faraday isolator; (*6*) Pockels cell; (*7*) high-reflection mirrors; (*8*) long-wavelength pass filter; (*9*) thin-rod active elements; (*10*) dumper; (*11*) quarter-wave plates; (*12*) curved mirrors; (*13*) pump laser diode bars.

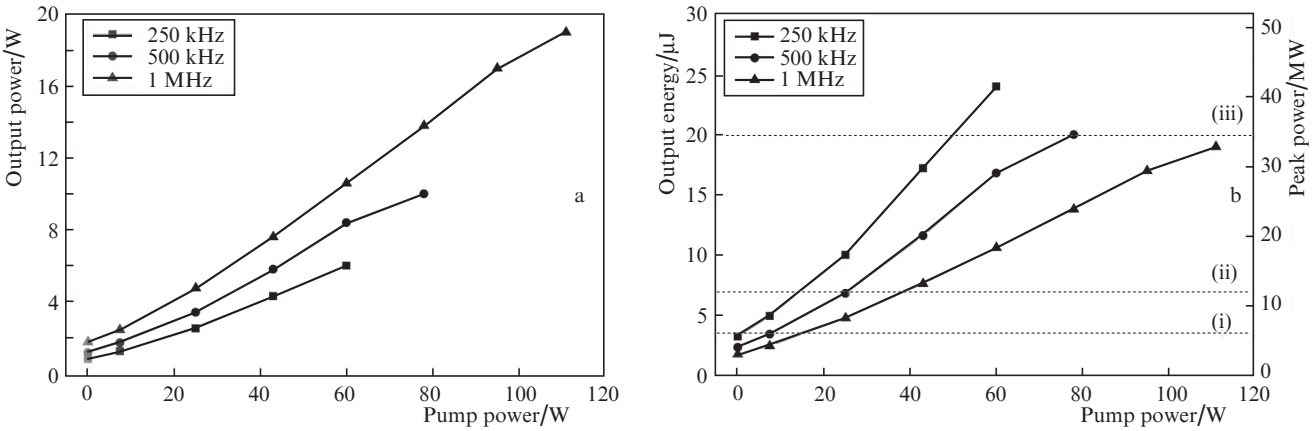

Figure 2. (a) Output power and (b) output energy and peak power vs. pump power of a second thin-rod amplifier with single-pass at 250 kHz, 500 kHz, and 1 MHz.

where n_0 and n_2 are the linear and nonlinear refractive indices [1, 9]. At a wavelength of 1030 nm, the critical power for a Yb:YAG crystal is approximately 1.3 MW. It is notable that the critical power does not depend on the beam size. By adjusting the beam diameter and divergence, as well as by optimising the crystal geometry, for example, by doping and choosing the length, critical damage can be prevented.

In an actual amplification system, even considering critical power, it is not easy to accurately predict the power at which the self-focusing becomes serious. Therefore, we performed experimental measurements to predict the nonlinear threshold at which the self-focusing becomes serious, using the property that the beam size changes greatly when nonlinearity occurs because of the lens effect. To visualise these effects, Fig. 3a shows how the beam profiles evolve as the output power increases at a repetition rate of 1 MHz. To compare with the case in which self-focusing is not serious due to low nonlinearity, the beam size was also measured at a repetition rate of 80 MHz with the same output power. The beam size was measured at a distance of ~1 m from the second amplifier. As can be seen from Fig. 3b, the beam diameters start to significantly differ at roughly an output power of 3.5 W, which corresponds to a pulse energy of 3.5 μJ and a peak power of 6 MW with a 580 fs pulse duration at a repetition rate of 1 MHz [6]. Even near 1.5 W which corresponds to a peak power of 2.5 MW, it can be seen that the beam size starts to increase slightly compared to the case of low nonlinearity, which shows a value similar to the calculated critical optical power of 1.3 MW.

Another way to estimate the importance of the self-focusing effect is the use of the B-integral [2], expressed as follows

$$B = \frac{2\pi}{\lambda}\int n_2 I(z)\,\mathrm{d}z\,. \tag{3}$$

Typically, B-integral values less than unity are recommended in the design of amplifiers to prevent the occurrence of self-focusing. A peak power of 6 MW corresponds to a B-integral of 0.4 at 1 MHz and 0.005 at 80 MHz, with a pulse duration of 580 fs, centre wavelength of 1030 nm, focused beam size of a 400 μm, and 19-mm-long Yb:YAG thin rod. Therefore, the experimentally measured threshold of self-focusing shows almost the same expectation value as with a critical power of 1.3 MW and a B-integral of 0.4. By using this measurement technique, we were able to predict system-dependent and accurate values for self-focusing in thin-rod media. It is notable that the pulse amplification with an excess of the critical power is possible without crystal damage, although the ampli-

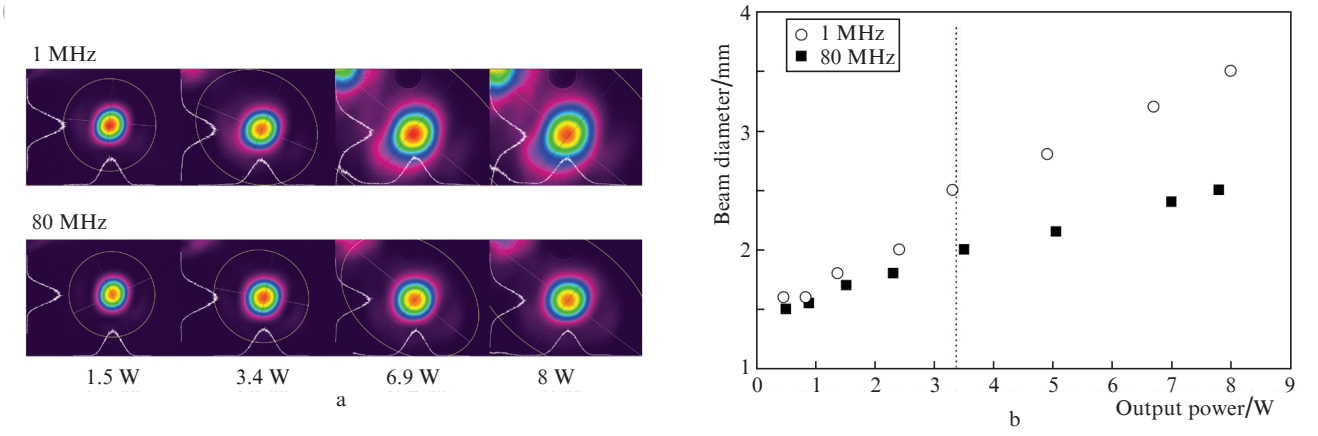

Figure 3. (Colour online) Measurement of the nonlinear threshold by comparing the beam size evolution of high (1 MHz) and low (80 MHz) pulse energy according to the amplification power: (a) beam profiles and (b) beam diameter vs. output power. The threshold of nonlinear effect is indicated in (b) by a vertical dotted line.

fied beam size is changed by self-focusing. This is because the beam collapses outside the crystal when the crystal length is shorter than the self-focusing length defined in Eqn (1).

Figure 4 shows one example of optical damage to a thin-rod crystal due to the self-focusing that we observed experimentally. The optical configuration of the laser system is shown [7] to be a three stage Yb:YAG thin-rod amplifier, with an average power up to more than 100 W with the CPA technique. In order to express the amplified output energy through the three-stage amplifier in one graph, the sum of the pump power accumulated through each amplifier is expressed as a total pump power. The three stage amplifier consists of the first and second TRA with a double-pass scheme and the third TRA with a single-pass scheme. The vertical line in Fig. 4 is drawn to distinguish each amplifier, and the peak power was measured with different repetition rates of 250 kHz, 500 kHz, and 1 MHz.

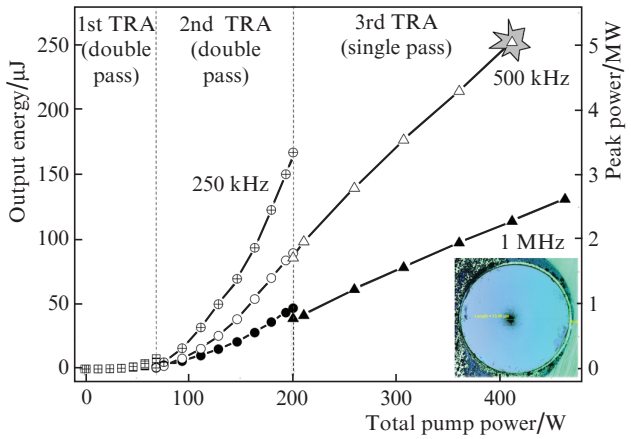

Figure 4. (Colour online) Output energy and peak power vs. total pump power in a three-stage Yb:YAG thin-rod system with CPA technique: Optical damage of the thin-rod crystal was observed at the peak power of 5 MW at 500 kHz. The inset shows the optically damaged crystal surface.

In the third stage with single-pass amplification, optical damage of the crystal facets is observed at an output energy of 250 μJ, which corresponds to a peak power of 5 MW. The peak power at which the damage occurred coincides well with the peak power threshold (6 MW) that we observed in Fig. 3. The damage of the crystal facet was due to the occurrence of self-focusing by the thermal lens with a pump power of 210 W, and not only due to the Kerr-lens effect. These results are in good agreement with those of a previous study [10].

An intensity-dependent refractive index called the Kerr effect also leads to spectral broadening in a nonlinear medium by self-phase modulation. Recently, great effort has been invested in the external nonlinear compression of laser pulses for ultrashort pulse duration through spectral broadening via self-phase modulation and subsequent chirp removal. There are various methods for nonlinear spectral broadening such as broadening of a dielectric waveguide, hollow-core fibre, multiple-plate, bulk medium, or multipass cell [11]. Among these options, spectral broadening in a bulk medium is a simple, robust, low-cost technique. It is used to focus an intense pulse into a bulk medium in which the self-focusing length is greater than that of a nonlinear medium [8].

In our experiments, we observed spectral broadening in a femtosecond laser system with a Yb:YAG thin-rod crystal (depicted in Fig. 5) when the pulse energy exceeded 12 MW, which corresponds to the dotted line (ii) in Fig. 2b. As the pulse energy increases, the spectrum near 1034 nm becomes stronger and shows asymmetry with a less powerful part shown in blue. Normally, according to the theory of self-phase modulation, SPM-induced spectral broadening predicts symmetric, multi-peaked spectra around the centre wavelength. Similar asymmetric spectral broadening has been observed and studied in previous research [8, 12–15].

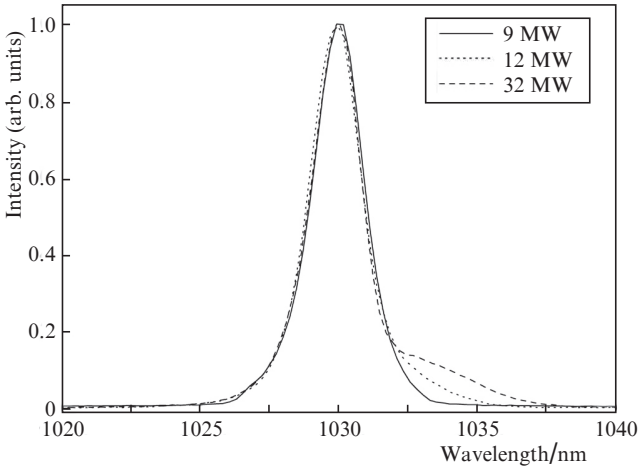

Figure 5. Experimentally observed spectral broadening due to the SPM in a femtosecond laser system with a Yb:YAG thin-rod crystal.

The asymmetric spectral broadening can be explained by several phenomena, such as high-order dispersion, chirped pulses, free carriers by two-photon absorption, or self-steepening [16, 17]. The asymmetric spectrum with a red shoulder cannot be explained by two-photon absorption generated free carriers. This is because free-carrier induced phase shifts cause asymmetric broadening of the spectra with a stronger blue part [16]. Moreover, the self-steepening effect can also be ruled out because the pulse duration at ~500 fs is not too short to consider self-steepening. Our spectral broadening shows a red shoulder, but no red shift [18].

For optical fibres, it is well known that asymmetry in the pulse shape that causes chirp would broaden the output spectrum asymmetrically [19]. We estimate that the chirped pulse is the main cause of the spectral asymmetry in our thin-rod amplification system. This is because the amplified pulses from the thin-rod amplifier undergo positive chirping through various dispersive materials, such as thin-rod active media as discussed elsewhere [6]. Moreover, a relatively high absorption coefficient of Yb:YAG near 1020–1025 nm (compared to 1035–1040 nm) could be a reason for asymmetric spectral broadening. It is meaningful to observe and study the spectral broadening that occurs more clearly with increasing output energy. Unfortunately, it was limited by the luminescence phenomena that occur when the pulse energy exceeds 20 μJ, as indicated by the dotted line (iii) in Fig. 2b. Moreover, a YAG crystal is not the proper material with which to study spectral broadening, compared to several wide band-gap materials. This is because a YAG crystal can easily be damaged before significant broadening due to impurities in the material [8].

Charge transfer (CT) luminescence is one kind of rare-earth luminescence. CT luminescence of a Yb-doped YAG

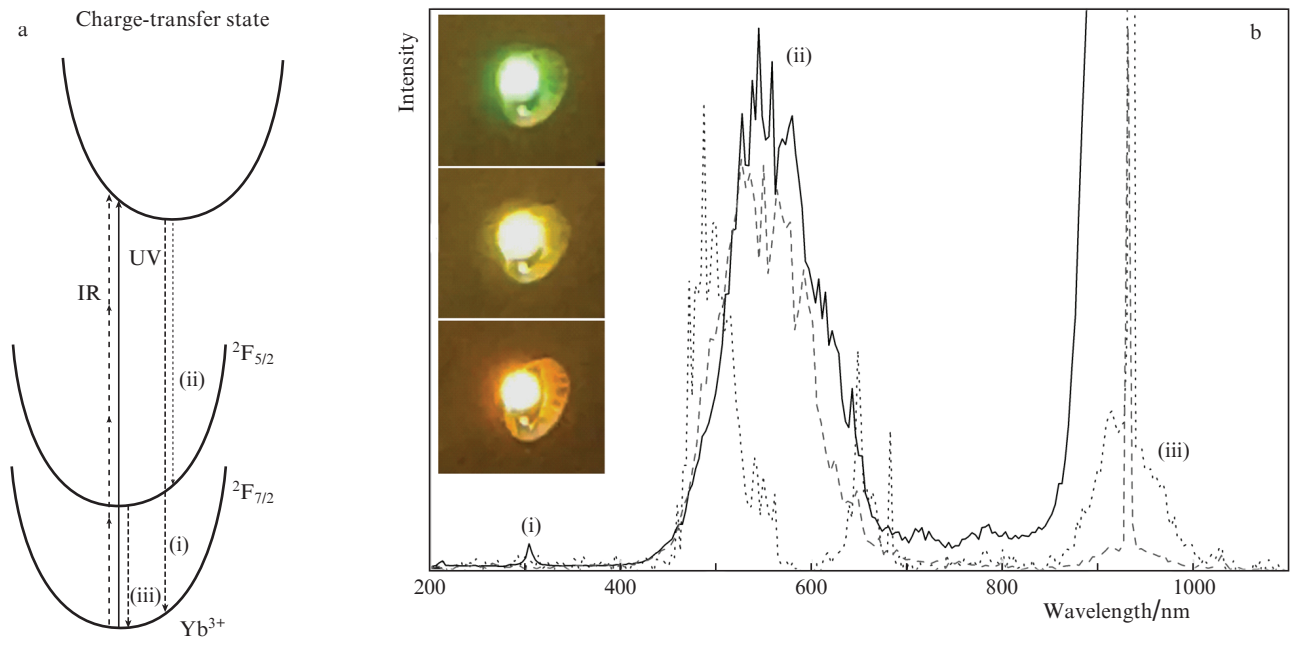

Figure 6. (Colour online) (a) Schematic of charge transfer luminescence in a Yb^{3+} ion and (b) emission spectrum of a Yb:YAG thin-rod crystal at a peak output power of 34 MW. The solid line corresponds to the spectrum measurement without a filter; dashed and dotted lines correspond to measurements with the visible band pass filter.

crystal can be observed because the CT state lies higher than the excited 4f states and the energy gap between the CT state and the highest excited state is large [20]. CT luminescence of Yb^{3+} has attracted broad attention due to possible applications as scintillation detectors in neutrino physics (e.g., solar neutrino detection, pulsed radiation detection, and space radiation detection). CT luminescence phenomena of Yb^{3+} ions in phosphate and oxysulfide lattices were first observed by Nakazawa [21]. A systematic study of CT luminescence from Yb^{3+} was investigated in a large variety of host crystals [22, 23]. Recently CT luminescence properties of Yb:YAG crystals were investigated and analysed [20, 24, 25].

Figure 6a shows the configuration coordinate diagram of CT luminescence processes with a curve diagram showing the potential energy. Yb^{3+} has an excited state ($^2F_{5/2}$) and the ground state ($^2F_{7/2}$) has ~10000 cm^{-1} energy separation between the two states. The CT state in Yb^{3+} that depends on the host mostly occurs at ~200–300 nm. Thus, the CT transitions usually observed have strong absorption in the UV range, which can be achieved not only through X-ray and UV excitation but also by NIR excitation involving multiphoton absorption [26, 27].

During Yb:YAG thin-rod amplification, we observed flashing light when the output peak power exceeded 34 MW. This was flickering of alternating colours: yellow, orange, and green (not white), as shown in Fig. 6b. The emission spectra of flashing light in a Yb:YAG thin rod was measured by a spectrometer without any filter as indicated by the solid line in Fig. 6b. The intensity saturation near 940 nm is due to transmission of the pump source through the thin-rod crystal. There are two peaks (~305 nm and ~560 nm) with broad emission bands, separated by roughly 10000 cm^{-1}, which shows the characteristics of CT luminescence of Yb^{3+}. These are commonly assigned to CT – $^2F_{7/2}$ and CT – $^2F_{5/2}$ transitions, which correspond to (i) and (ii) in Fig. 6. Through the visible bandpass filter (dashed and dotted line), broad emission near 930 nm (corresponding to the transition $^2F_{5/2} - {}^2F_{7/2}$) can be visualised [(iii) in Fig. 6], despite the fact that there is still intensity saturation of the pump light near 940 nm. The observed CT luminescence was achieved through infrared (IR) excitation via multiphoton absorption with at least 4–5 IR photons. This is possible due to the intense power peak generated in the thin-rod crystal by self-focusing of ultrashort pulses. The relative intensity between each transition depends on the impurities in the material, the temperature of the environment, and the excitation wavelength [20, 24, 25].

3. Frequency conversion with a Yb:YAG thin-rod fs amplifier

When a strong electric field that originates from an incident pulse is applied to a nonlinear medium, it induces nonlinear polarisation that can be ignored in the linear regime. Among the nonlinearities that appeared, part of the components proportional to the amplitude of an electric field contributes to the frequency conversion. Frequency conversion is one representative nonlinear phenomenon based on second-order nonlinearity. Second harmonic generation (SHG) is generation of a second harmonic frequency of 2ω from incident frequency of ω in a nonlinear medium. Sum frequency generation (SFG) involves generation of a new frequency component ω_3, which is the sum of the incident frequencies ω_1 and ω_2 [28]. In this research, frequency doubling and tripling are achieved by SHG of the fundamental beam and SFG of the fundamental and SHG beams, as shown in Fig. 7. For frequency tripling with high conversion efficiency, SFG is generally adopted instead of third harmonic generation based on third-order nonlinearity. Experimentally, it is important to optimise the peak intensity by controlling the beam waist in the nonlinear medium in regards to the fixed pulse energy, pulse duration, and medium length. In this Section, we discuss the frequency conversion of SHG for 515 nm and SFG for 343 nm wave-

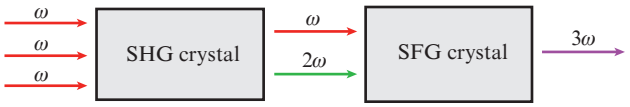

Figure 7. Diagram of frequency doubling and tripling.

lengths generated from a Yb:YAG thin-rod femtosecond amplifier with the pulse energy of ~260 nJ.

For the SHG and SFG experiments, a mode-locked Yb:KGW oscillator is directly amplified by a Yb:YAG thin-rod amplifier. The master oscillator (MO) is similar to the model in our previous research. It provides a maximum output power of 2 W, centre wavelength of 1030.5 nm, spectral bandwidth of 7.5 nm, repetition rate of 80 MHz, and pulse duration of 170 fs [29, 30]. The pulse generated from the MO is incident onto the Yb:YAG thin-rod amplifier, which is similar to the model described above. The amplified pulse exhibits an output power of 20.9 W, centre wavelength of 1030.3 nm, and spectral bandwidth of 3.0 nm. To decrease the pulse duration, a chirp mirror of –10000 fs^2 per bounce was adopted. Assuming a sech^2 shaped pulse, the pulse duration decreased from 442 to 364 fs by applying a negative dispersion value (–30000 fs^2). With a minimum pulse duration of 364 fs, a peak power of 631.6 kW is achieved.

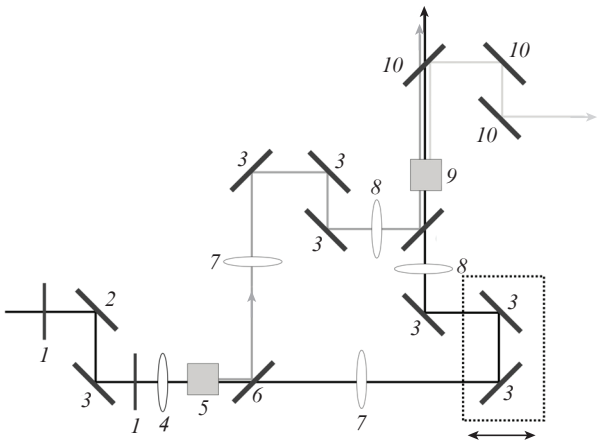

Figure 8. Schematic of a frequency doubling and tripling system: (*1*) half-wave plate; (*2*) thin-film polariser; (*3*) high-reflectivity mirror; (*4*) focusing lens for SHG; (*5*) BBO crystal for SHG; (*6*) beam splitter for SHG; (*7*) collimating lens for SFG; (*8*) focusing lens for SFG; (*9*) BBO crystal for SFG; (*10*) beam splitter for SFG.

A schematic of the frequency doubling and tripling system is shown in Fig. 8. A SHG crystal [6 × 6 × 2 mm, $\theta = 23.4°$, $\varphi = 90°$; BBO: β-BaB_2O_4, beta barium borate, type I (ooe), Castech] was used for frequency doubling. To control the output power of the incident fundamental beam, a combination of half-wave plate and thin-film polariser was adopted. To change the size of the incident beam, convex lenses with focal lengths 100, 150, and 200 mm were used. The focused beam areas were 3701, 7380, and 16036 μm^2, corresponding to the focal lengths of 100, 150, and 200 mm, respectively. The generated SHG and residual fundamental beam were divided by a separator that exhibits high reflection near 515 nm for s-polarisation and high transmission near 1030 nm for p-polarisation.

For frequency tripling, the spatial walk-off and temporal walk-off originating from the SHG should be controlled to optimise conversion efficiency because of the relatively low pulse energy (~100 nJ). The SHG beam and remaining fundamental beam from the SHG crystal were divided by a beam splitter that exhibits high reflection near 515 nm and high transmission near 1030 nm. The separated beams were collimated by an AR coated convex lens ($f = 300$ mm). For control of the focused beam size, a set of AR-coated convex lenses of focal lengths 150, 200, and 250 mm was used for each beam line. The focused beams were combined by the SHG beam splitter and then spatially overlapped in the SFG crystal. As a SFG crystal, BBO [3 × 3 × 6 mm, $\theta = 40°$, $\varphi = 30°$, type II (eoe), Castech] was used. The SFG beam was reflected by three beam splitters for SFG, which exhibited high reflection at 343 nm for p-polarisation and high transmission at 1030 nm for p-polarisation and 515 nm for s-polarisation. They eliminated the fundamental and SHG beams. To minimise the temporal walk-off, a delay line was inserted in the fundamental beam line and the delay was precisely controlled by the SFG output power.

The output power of the SHG is shown in Fig. 9a. With a seed power of 20.9 W, maximum SHG output powers of 11.1, 10.4, and 7.9 W were achieved at focal lengths of 100, 150, and 200 mm, respectively. The output power and conversion efficiency of the SHG as functions of the beam area are shown in Fig. 9b. It is confirmed that the beams of smaller size exhibit a higher SHG output power and conversion efficiency. With $f = 100$ mm, maximised conversion efficiency is exhib-

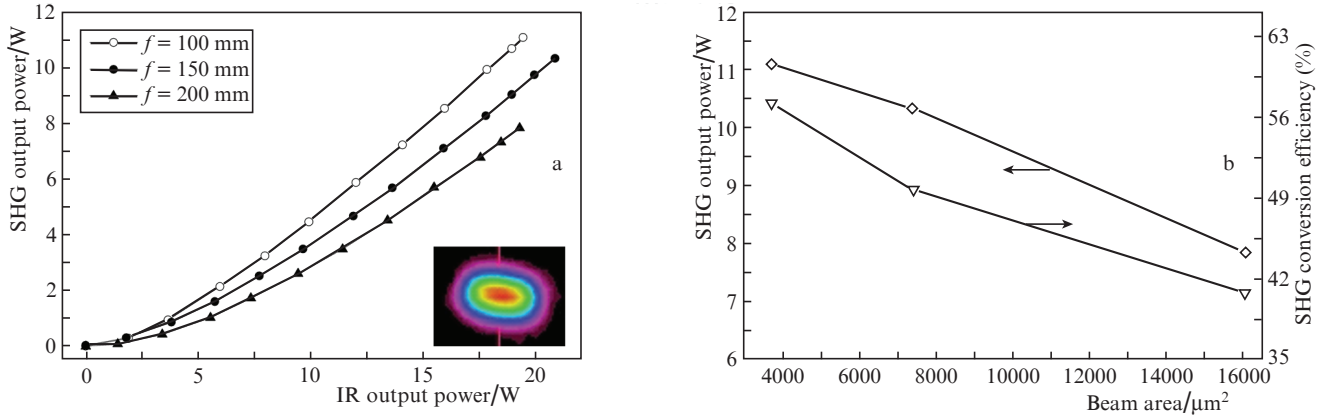

Figure 9. (Colour online) (a) Experimentally measured SHG output power vs. incident IR power (the inset shows the SHG beam profile for $f = 150$ mm), and (b) maximum output power and conversion efficiency vs. focused beam area in the SHG crystal.

Table 1. SHG parameters from the Yb:KGW oscillator and Yb:YAG thin-rod amplifier.

Source	Nonlinear-medium	P_{out}/W	F_{rep}/MHz	E_p/nJ	τ/fs	P_p/kW	A/cm^2	I_p/GW cm^{-2}	P_{SHG}/W	η (%)	Refs
Yb:KGW oscillator (MO)	BBO (2 mm)	1.1	80	13.8	175	69.1	6.16×10^{-6}	22.4	0.56	50.9	[31]
Yb:KGW oscillator (MO) + Yb:YAG thin-rod amplifier	BBO (2 mm)	20.9	80	261.3	364	631.6	7.38×10^{-5}	17.1	10.4	49.7	This work

Note: P_p is the peak power; A is the focused beam area; I_p is the peak intensity; P_{SHG} is the SHG output power; η is the conversion efficiency.

ited along with the output power, but the beam shape is elliptical due to the spatial walk-off in the SHG crystal, which is not good for frequency tripling. With f = 150 mm, a maximum SHG output power of 10.4 W and conversion efficiency of 49.7% are confirmed by the clean beam profile shown in the inset of Fig. 9a. Thus, the case of f = 150 mm was chosen for the SFG of the UV beam. Table 1 summarises the SHG parameters of the Yb:KGW oscillator from our previous work and of the Yb:YAG thin-rod amplifier seeded by the Yb:KGW oscillator [31]. From these parameters, the peak intensity of the fundamental beam in the nonlinear medium was calculated to be 22.4 GW cm^{-2} for the MO and 17.1 GW cm^{-2} for the thin-rod amplifier. Because of the relatively high pulse energy compared to the MO, the beam size in the nonlinear medium could be increased and effectively decrease the spatial walk-off with sufficient conversion efficiency of 49.7%.

The SHG spectrum corresponding to f = 150 mm is shown in Fig. 10a, and a centre wavelength of 515.1 nm and a spectral bandwidth of 1.9 nm are confirmed. The corresponding pulse duration is shown in Fig. 10b. Assuming a sech^2 shaped pulse, the SHG pulse duration was determined to be 280 fs with a time bandwidth product of 0.6. This relatively large time bandwidth product value originated from the resolution limit spectrometer of ~0.75 nm. The pulse duration decreased compared to the pulse duration of a fundamental beam of 364 fs. This is because the intensity of the SHG is proportional to the square of the intensity of the fundamental beam. Assuming a Gaussian beam, the square term is the same as the factor $1/\sqrt{2}$ of pulse duration. Our experimental result shows that the ratio of pulse durations between the fundamental and SHG beams is ~0.77, which is close to $1/\sqrt{2}$.

The SFG output power as a function os the output power of the fundamental beam is shown in Fig. 11a. The maximum

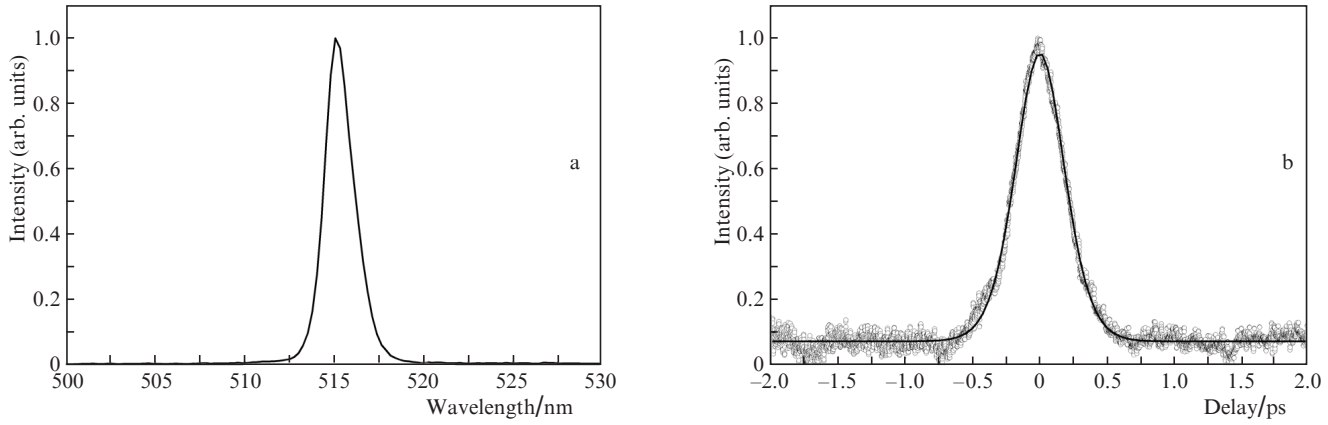

Figure 10. (a) Experimentally measured SHG spectrum and (b) corresponding autocorrelation function.

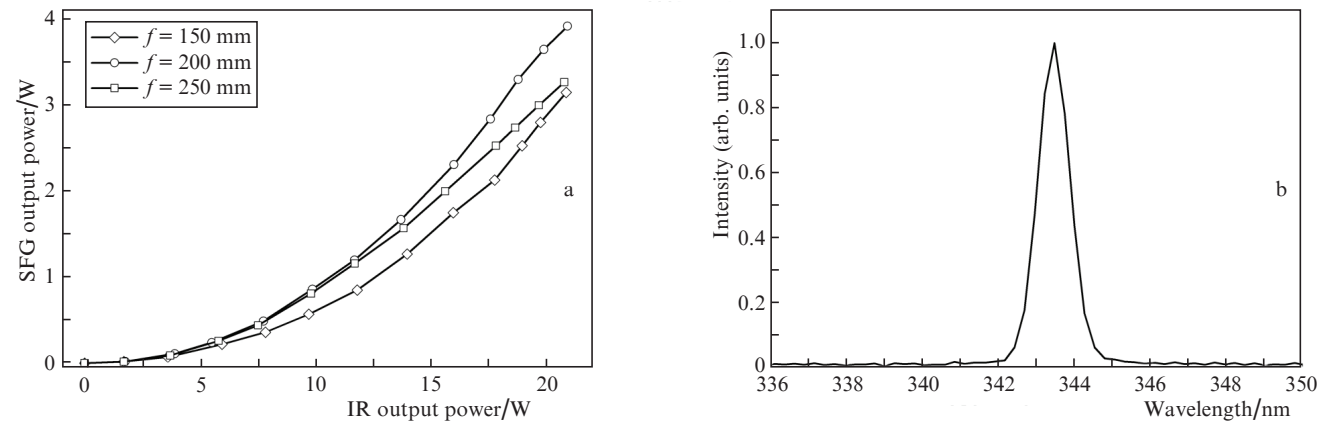

Figure 11. (a) Experimentally measured SFG output power as a function of incident IR power and (b) spectrum corresponding to the maximum output power of 3.92 W.

Table 2. SFG parameters for the Yb:YAG thin-rod amplifier.

Focal length/mm	Focused beam area at 1030 nm/cm^2	Focused SHG beam area/cm^2	Peak intensity at 1030 nm/GW cm^{-2}	SHG peak intensity/GW cm^{-2}	SFG output power/W	η (%)
150	2.74×10^{-5}	2.52×10^{-5}	23.2	32.4	3.2	15.3
200	3.84×10^{-5}	4.23×10^{-5}	16.5	19.3	3.9	18.7
250	6.94×10^{-5}	7.03×10^{-5}	9.1	11.6	3.3	15.8

output power corresponding to the focusing lens with $f = 150$, 200, and 250 mm is 3.15, 3.92, and 3.27 W, respectively. The SFG spectrum at a maximum output power is shown in Fig. 11b, with a centre wavelength and spectral bandwidth being measured to be 343.5 and 1.0 nm, respectively. Table 2 exhibits the SFG parameters with the Yb:YAG thin-rod amplifier. The peak intensity of the fundamental and SHG beams in the SFG crystal is 23.2 and 32.4 GW cm^{-2} for $f = 150$; 16.5 and 19.3 GW cm^{-2} for $f = 200$ mm; and 9.1 and 11.6 GW cm^{-2} for $f = 250$ mm. The SFG conversion efficiencies of 15.3%, 18.7%, and 15.8% corresponds to focal lengths of 150, 200, and 250 mm, respectively. From this experiment, the spatial walk-off was minimised at $f = 200$ mm, which shows the beam area of the fundamental and SHG beams of 3.84×10^{-5} and 4.23×10^{-5} cm^2.

In cases with a relatively high pulse energy (over hundreds of μJ), the conditions for spatial walk-off and temporal walk-off can be reduced due to the relatively large beam size, with a sufficiently high peak intensity [32]. In the case of a relatively low pulse energy (on the order of hundreds of nJ), it is necessary to decrease the beam size in the nonlinear medium. This requires more careful compensation for the spatial and temporal walk-off. In this research, the spatial and temporal walk-off were compensated for separately and the condition for frequency tripling from the Yb:YAG thin-rod femtosecond amplifier was optimised with an output power of 3.9 W and NIR/UV conversion efficiency of 18.7%. After considering various experimental environments, we hope that our research has great meaning as a reference on frequency doubling and tripling of femtosecond pulses with pulse energy levels of hundreds of nJ.

4. Conclusions

In this research, various nonlinear phenomena which can appear during amplification process in a femtosecond laser system based on Yb:YAG thin-rod are studied.

Firstly, it is shown that the lowest nonlinear threshold is the optical Kerr effect. This effect leads to self-focusing of the radiation, causing deterioration of the angular divergence and damage of the active materials in the laser system. To avoid these phenomena, the breakup integral should be limited to the value $B < 1$. At such values of B, self-phase modulation, which is another effect limiting the peak power of radiation in some cases, does not appear. Another nonlinear effect, charge transfer luminescence observed in Yb:YAG crystals, caused by multiphoton absorption of laser radiation, may be one of the origins for limiting the peak power scaling of laser system.

In addition, a study was carried out on the frequency conversion of femtosecond laser pulses during its doubling ($\lambda = 515$ nm) and tripling ($\lambda = 343$ nm). By optimising the conversion scheme, efficiencies of about 50% were obtained when generating the second harmonic and about 19% when generating the sum frequency.

We hope it is meaningful to experimentally show that the Kerr effect is the most influential factor for limiting the radiation power in a laser system on Yb:YAG thin rods. Also the results of optimisation and quantification of frequency conversion will be helpful for the research of frequency conversion of hundred-nJ-level of pulse energy.

Acknowledgements. The authors are grateful to O.V. Palashov, I.B. Mukhin, and I.I. Kuznetsov from the Institute of Applied Physics of the Russian Academy of Sciences for providing amplifying modules.

This research was supported by Korea Electrotechnology Research Institute (KERI) Primary Research Programme through the National Research Council of Science & Technology (NST) funded by the Ministry of Science and ICT (MSIT) (No. 21A01024).

References

1. Diels J., Rudolph W. *Ultrashort Laser Pulse Phenomena* (Elsevier, 2006).
2. Weiner A.M. *Ultrafast Optics* (Hoboken, NJ: Wiley, 2009).
3. Lesparre F., Gomes J.T., Délen X., Martial I., Didierjean J., Pallmann W., Resan B., Eckerle M., Graf T., Ahmed M.A., Druon F., Balembois F., Georges P. *Opt. Lett*., **40**, 2517 (2015).
4. Markovic V., Rohrbacher A., Hofmann P., Pallmann W., Pierrot S., Resan B. *Opt. Express*, **23**, 25883 (2015).
5. Kuznetsov I., Mukhin I., Palashov O., Ueda K.-I. *Opt. Lett*., **43**, 3941 (2018).
6. Yang J., Lee B., Kim J.W., Jeong B., Sall E.G., Chizhov S.A., Heo D., Yashin V.E., Kim G.H. *Quantum Electron*., **49**, 1168 (2019) [*Kvantovaya Elektron*., **49**, 1168 (2019)].
7. Yang J., Kim J.W., Sall E.G., Lee B., Jeong B., Park S., Kim C., Yashin V.E., Kim G.H. *Quantum Electron*., **51**, 873 (2021) [*Kvantovaya Elektron*., **51**, 873 (2021)].
8. Seidel M., Arisholm G., Brons J., Pervak V., Pronin O. *Opt. Express*, **24**, 9412 (2016).
9. Fibich G., Gaeta A.L. *Opt. Lett*., **25**, 335 (2000).
10. Pouysegur J., Weichelt B., Guichard F., Zaouter Y., Hönninger C., Mottay E., Druon F., Georges P. *Opt. Express*, **24**, 9896 (2016).
11. Weitenberg J., Vernaleken A., Schulte J., Ozawa A., Sartorius T., Pervak V., Hoffmann H.-D., Udem T., Russbüldt P., Hänsch T.W. *Opt. Express*, **25**, 20502 (2017).
12. Hsieh I.-W., Chen X., Dadap J.I., Panoiu N.C., Osgood R.M., McNab S.J., Vlasov Y.A. *Opt. Express*, **14**, 12380 (2006).
13. Dannecker B., Negel J.-P., Loescher A., Oldorf P., Reichel S., Peters R., Graf T., Ahmed M.A. *Opt. Commun*., **429**, 180 (2018).
14. Gröbmeyer S., Firtsch K., Schneider B., Poetzlberger M., Pervak V., Brons J., Pronin O. *Appl. Phys. B*, **126**, 159 (2020).
15. Sun D., Guo J., Wang W., Du X., Gao Y., Gao Z., Liang X. *IEEE Photonics J*., **13**, 1 (2021).
16. Dulkeith E., Vlasov Y.A., Chen X., Panoiu N.C., Osgood R.M. *Opt. Express*, **14**, 5524 (2006).
17. Modotto D., Mondia J.P., Linden S., Tan H.W., Morandotti R., Kleckner T.C., Locatelli A., Angelis C.D., Driel H.M., Stanley C.R., Aitchison J.S. *Opt. Commun*., **249**, 201 (2005).
18. Moses J., Malomed B.A., Wise F.W. *Phys. Rev. A*, **76**, 021802 (2007).
19. Stolen R.H., Lin C. *Phys. Rev. A*, **17**, 1448 (1978).
20. Rydberg S., Engholm M. *J. Appl. Phys*., **113**, 223510 (2013).
21. Nakazawa E. *Chem. Phys. Lett*., **56**, 161 (1978).

22. Pieterson L., Heeroma M., Heer E., Meijerink A. *J. Lumin.*, **91**, 177 (2000).
23. Nikl M., Yoshikawa A., Fukuda T. *Opt. Mater.*, **26**, 545 (2004).
24. Guerassimova N., Garnier N., Dujardin C., Petrosyan A.G., Pedrini C. *J. Lumin.*, **94**, 11 (2001).
25. Zhu M., Qi H., Pan M., Hou Q., Jiang B., Jin Y., Han H., Song A., Zhang H. *J. Cryst. Growth*, **490**, 51 (2018).
26. Wang J., Hao J.H., Tanner P.A. *Opt. Lett.*, **35**, 3922 (2010).
27. Verma R.K., Rai S.B. *Chem. Phys. Lett.*, **559**, 71 (2013).
28. Sutherland R.L. *Handbook of Nonlinear Optics* (New York: CRC Press, 2003) pp 33 – 34.
29. Kim G. H., Yang J., Lee D.S., Kulik A.V., Sall E.G., Chizhov S.A., Yashin V.E., Kang U. *Quantum Electron.*, **42**, 292 (2012) [*Kvantovaya Elektron.*, **42**, 292 (2012)].
30. Kim J.W., Sall E.G., Lee B., Jeong B., Park S., Kim C., Heo D., Yashin V.E., Yang J., Kim G.H. *Opt. Express*, **27**, 31418 (2019).
31. Kim D.J., Park E.J., Lee B., Chizhov S.A., Sall E.G., Kim J.W., Kim G.H., Kim J.W. *Jpn. J. Appl. Phys.*, **57**, 122702 (2018).
32. Rothhardt J., Rothhardt C., Müller M., Klenke A., Kienel M., Demmler S., Elsmann T., Rothhardt M., Limpert J., Tünnermann A. *Opt. Lett.*, **41**, 1885 (2016).